Development of Calculation and Analysis Methods for the Dynamic First Hyperpolarizability Based on the Ab Initio Molecular Orbital − Quantum Master Equation Method

ARTICLE *in* THE JOURNAL OF PHYSICAL CHEMISTRY A · APRIL 2012

Impact Factor: 2.69 · DOI: 10.1021/jp301213z · Source: PubMed

8 AUTHORS, INCLUDING:

Ryohei Kishi
Osaka University
110 PUBLICATIONS **1,955** CITATIONS
SEE PROFILE

Yasuteru Shigeta
University of Tsukuba
174 PUBLICATIONS **1,836** CITATIONS
SEE PROFILE

Masayoshi Nakano
Osaka University
337 PUBLICATIONS **4,793** CITATIONS
SEE PROFILE

THE JOURNAL OF PHYSICAL CHEMISTRY A

Article

pubs.acs.org/JPCA

Development of Calculation and Analysis Methods for the Dynamic First Hyperpolarizability Based on the Ab Initio Molecular Orbital − Quantum Master Equation Method

Ryohei Kishi,* Hiroaki Fujii, Shingo Kishimoto, Yusuke Murata, Soichi Ito, Katsuki Okuno, Yasuteru Shigeta, and Masayoshi Nakano*

Department of Materials Engineering Science, Graduate School of Engineering Science, Osaka University, Toyonaka, Osaka 560-8531, Japan

Supporting Information

ABSTRACT: We develop novel calculation and analysis methods for the dynamic first hyperpolarizabilities β [the second-order nonlinear optical (NLO) properties at the molecular level] in the second-harmonic generation based on the quantum master equation method combined with the ab initio molecular orbital (MO) configuration interaction method. As examples, we have evaluated off-resonant dynamic β values of donor (NH_2)- and/or acceptor (NO_2)-substituted benzenes using these methods, which are shown to reproduce those by the conventional summation-over-states method well. The spatial contributions of electrons to the dynamic β of these systems are also analyzed using the dynamic β density and its partition into the MO contributions. The present results demonstrate the advantage of these methods in unraveling the mechanism of dynamic NLO properties and in building the structure−dynamic NLO property relationships of real molecules.

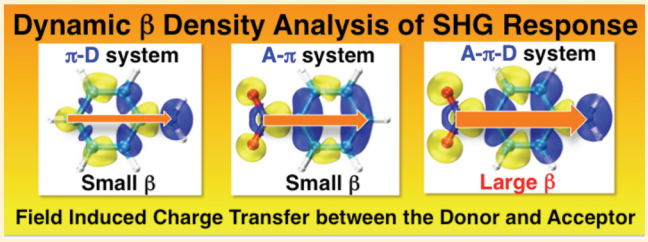

1. INTRODUCTION

Molecular materials exhibiting large second-order nonlinear optical (NLO) responses have attracted much attention in molecular science and engineering owing to their feasibility of manipulating laser beams and their applications in electro-optical data processing and innovative all-optical technologies such as the frequency conversion technique of laser light.[1,2] The second-order NLO response of molecular materials is characterized by the second-order nonlinear susceptibility, which originates in the first hyperpolarizability β of constituent molecules. On the other hand, in the field of nonlinear optical spectroscopy, first hyperpolarizability is known as one of the most fundamental molecular properties, which describes, for example, hyper-Rayleigh scattering (HRS), sum-frequency generation (SFG), and second-harmonic generation (SHG). Experimental and theoretical analyses of these phenomena based on the observation and computation are therefore indispensable for understanding detailed electronic, vibrational, and rotational structures of molecules.[3,4] In the field of materials science, enormous efforts have so far been put into the quest for novel molecular structures possessing a large amplitude of β.[2] Not only experimental but also theoretical methods based on the electronic structure theory have been applied to the clarification of the structure−property relationship, which is indispensable for rational design of such NLO-active molecules. This indicates that the realization of highly efficient second-order NLO materials is closely related to the development of theoretical and experimental techniques.

On the theoretical side, there have been several different methods proposed for the calculation and analysis of frequency-dependent (dynamic) β. The summation-over-states (SOS) method based on the time-dependent perturbation theory gives an analytic expression for dynamic β in terms of the excitation energies and properties among the electronic states.[5] The SOS method also offers very useful approximate expressions for dynamic β, where only a few significant charge-transfer (CT) excited states are taken into account. Several other methods giving analytical methods for dynamic β, for example, the time-dependent Hartree−Fock/Kohn−Sham (TD-HF/KS) schemes,[6] the response theory methods,[7,8] and the quasi-energy derivative methods,[9] have also succeeded in directly evaluating dynamic β of several molecular systems. The advantage of employing these methods exists in their direct (without time evolution of the system) and highly accurate evaluation features of arbitrary high-order response properties in several quantum chemical methods taking account of electron correlation effects, which are essential for the quantitative description of dynamic β.

On the other hand, numerical methods treating real-time evolution of electron density based on the quantum chemical calculations have recently been developed with the aim of simulating several excitation and carrier transfer dynamics in

Received: February 7, 2012
Revised: March 28, 2012
Published: April 2, 2012

dx.doi.org/10.1021/jp301213z | J. Phys. Chem. A 2012, 116, 4371−4380

small, super-, and supramolecules and solids.[10−17] These methods can directly track the spatio-temporal evolution of electron density and thus have the advantage of revealing the detailed structure−property relations of such dynamic phenomena. Because the NLO response signals result from the field-induced dynamics of the electron density, such real-time numerical methods are also expected to be useful for giving a new chemical and physical insight into the structure−property relationships of dynamic β. Indeed, there have been several studies of the dynamic hyperpolarizabilities based on the real-time simulation of electron dynamics using the numerical Liouville equation approach (NLA) with a definition of nonperturbative (hyper)polarizability[18] and the time-dependent density functional theory (TDDFT) method.[19] As an extension of the NLA, we have developed the quantum master equation (QME) method combined with the ab initio molecular orbital (MO) configuration interaction singles (CIS), which is referred to as the MOQME method.[20] We have applied the MOQME method to the real-time simulations of exciton (electron−hole pair) transfer dynamics in supermolecules and molecular aggregates and have clarified the mechanisms of coherent and incoherent energy-transfer processes.[21] We have also extended the MOQME method so as to evaluate the dynamic polarizability α of open-shell systems by combining with the spin-unrestricted TDDFT method within the Tamm−Dancoff approximation.[22] In this study, we further present the calculation scheme for dynamic β in the SHG based on the MOQME method combined with the numerical calculation scheme of nonperturbative hyperpolarizability in the NLA.[18] For analysis of dynamic β, we provide a calculation scheme of the doubled-frequency response part of the electron density, that is, the dynamic β density,[23] based on the MOQME method. The map of a dynamic β density illustrates the spatial contributions of the one-electron reduced density to the dynamic β. Performance of the present methods is demonstrated in the dynamic β of typical donor (NH_2)- and/or acceptor (NO_2)-substituted benzenes, that is, aniline, nitrobenzene, and 4-nitroaniline. To confirm the reliability of these numerical methods, the calculated results of dynamic β in the off-resonant condition are compared with those calculated by the conventional SOS method. We then reveal the spatial SHG response of the one-electron reduced density as well as the effects of introducing donor and/or acceptor substitution groups using the dynamic β density maps. The present calculation and analysis methods based on the MOQME are expected to contribute to the clarification of detailed structure−property relationships and the construction of rational design guidelines toward efficient dynamic second-order NLO molecules.

2. METHODOLOGY

2.1. MOQME Method. We briefly explain the MOQME method for the time evolution of the system reduced density matrix (RDM).[20] The one-exciton eigenstates are calculated by the CIS method. We assume that the one-exciton basis is described by the single-excitation configurations, $\{|\Psi_a^r\rangle\} = \{|i(= \psi_a \rightarrow \psi_r)\rangle\}$, where ψ_a and ψ_r are the occupied and virtual MOs, respectively. On the basis of the CIS method, each exciton eigenstate $|\alpha\rangle$ with eigenfrequency ω_α is expanded using the exciton basis $|i\rangle$

$$|\alpha\rangle = \sum_i |i\rangle\langle i|\alpha\rangle = \sum_i C_{i\alpha}|i\rangle \tag{1}$$

where $C_{i\alpha}$ is the CI coefficient. The QME method can treat the time evolution of the system RDM, $\rho(t)$, in the presence of the system−bath interaction. According to the standard method of relaxation theory,[24−26] we trace over the phonon bath states, which are assumed to be in the thermal equilibrium state at temperature T, and thus derive the QME for the system RDM in the Born−Markov approximation[26]

$$\frac{d\rho_{\eta\lambda}}{dt} = -i(\omega_\eta - \omega_\lambda)\rho_{\eta\lambda} - \sum_{\sigma\nu}^{M} \Gamma_{\eta\lambda;\sigma\nu}\rho_{\sigma\nu} - F^l \sum_{\sigma}^{M} (\mu^l_{\eta\sigma}\rho_{\sigma\lambda} - \rho_{\eta\sigma}\mu^l_{\sigma\lambda}) \qquad (\eta \neq \lambda) \tag{2}$$

$$\frac{d\rho_{\eta\eta}}{dt} = -\sum_{\lambda}^{M} \Gamma_{\eta\eta;\lambda\lambda}\rho_{\lambda\lambda} - F^l \sum_{\lambda}^{M} (\mu^l_{\eta\lambda}\rho_{\lambda\eta} - \rho_{\eta\lambda}\mu^l_{\lambda\eta}) \tag{3}$$

where M gives the number of states involving the ground and excited states. F^l indicates a laser amplitude in the l direction, and μ^l represents the lth component of the transition moment between the states. Here, one exciton, that is, an electron−hole pair, is assumed to be described by a single excitation ($a \rightarrow r$) caused by the irradiation of a linear polarized continuous wave (cw) laser field F. Γ determines the relaxation factor between the RDM matrix elements originating in the exciton−phonon coupling. The time evolution of system polarization $P^l(t)$ is calculated from the system RDM by $P^l(t) = \mathrm{tr}[\mu^l\rho(t)] \equiv \int \rho_{\mathrm{pol}}(\boldsymbol{r},t)(-r^l)\,d\boldsymbol{r}$, where we define the polarization density as $\rho_{\mathrm{pol}}(\boldsymbol{r},t) \equiv \rho(\boldsymbol{r},t) - \rho(\boldsymbol{r},0)$. The system RDM $\{\rho_{\eta\lambda}(t)\}$ in the state basis obtained by numerically solving eqs 2 and 3 is then converted into that $\{\rho_{ij}(t)\}$ in the one-exciton basis $\{|i\rangle\}$. In the present case, $\rho(\boldsymbol{r},0)$ is represented by the one-electron reduced density of the Hartree−Fock ground state. Therefore, we can represent the polarization density as[20b]

$$\begin{aligned}\rho_{\mathrm{pol}}(\boldsymbol{r},t) &\equiv \rho(\boldsymbol{r},t) - d_{11}(\boldsymbol{r}) \\ &= \sum_{i(\neq 1)} [d_{ii}(\boldsymbol{r}) - d_{11}(\boldsymbol{r})]\rho_{ii}(t) \\ &\quad + 2\sum_{i=2} d_{1i}(\boldsymbol{r})\,\mathrm{Re}[\rho_{1i}(t)] \\ &\quad + 2\sum_{i<j(i,j\neq 1)} d_{ij}(\boldsymbol{r})\,\mathrm{Re}[\rho_{ij}^{\mathrm{real}}(t)]\end{aligned} \tag{4}$$

where $d_{ij}(\boldsymbol{r})$ are the one-electron reduced density matrices in the one-exciton basis $\{|i\rangle\}$. The superscript "real" means the real part of the density matrices. Because each $|i\rangle$ corresponds to the single excitation configuration, we can rewrite $d_{ij}(\boldsymbol{r})$ by using the occupied $\{\psi_a(\boldsymbol{r}),\psi_b(\boldsymbol{r}),...\}$ and virtual $\{\psi_r(\boldsymbol{r}),\psi_s(\boldsymbol{r}),...\}$ orbitals. As a result, we obtain the following expression for $\rho_{\mathrm{pol}}(\boldsymbol{r},t)$[20b]

$$\begin{aligned}\rho_{\mathrm{pol}}(\boldsymbol{r},t) &= \sum_{i(a\rightarrow r)=2} [(|\psi_r(\boldsymbol{r})|^2 - |\psi_a(\boldsymbol{r})|^2)\rho_{ii}(t) \\ &\quad + 2\sqrt{2}\psi_a(\boldsymbol{r})\psi_r(\boldsymbol{r})\,\mathrm{Re}[\rho_{1i}(t)] \\ &\quad + 2\sum_{j(a\rightarrow s)(>i)} \psi_r(\boldsymbol{r})\psi_s(\boldsymbol{r})\,\mathrm{Re}[\rho_{ij}(t)] \\ &\quad - 2\sum_{j(b\rightarrow r)(>i)} \psi_a(\boldsymbol{r})\psi_b(\boldsymbol{r})\,\mathrm{Re}[\rho_{ij}(t)]]\end{aligned} \tag{5}$$

dx.doi.org/10.1021/jp301213z | J. Phys. Chem. A 2012, 116, 4371−4380

2.2. Calculation Scheme of Dynamic β and Its Density.

From the nonperturbative definition of hyperpolarizabilities,[18,23b,d] the diagonal l-axis component of dynamic β ($=\beta_{lll}$) in the SHG (in B-convention[27]) is expressed as

$$\beta_{lll}(-2\omega;\,\omega,\,\omega) = \frac{P^l(2\omega)}{4\varepsilon^l(\omega)\varepsilon^l(\omega)} \tag{6}$$

where $\varepsilon^l(\omega)$ and $P^l(2\omega)$ represent the external field and system polarization in the frequency domain obtained by the Fourier transform of $F^l(t)$ [$=2\varepsilon^l(\omega)(e^{i\omega t} + e^{-i\omega t})$] and $P^l(t)$, respectively. In general, $P^l(2\omega)$ obtained from the QME method involves not only the second-order but also the higher-order components of responses. The dynamic β in the nonperturbative definition approximately coincides with that in the perturbative definition (e.g., calculated by the SOS method) when we can neglect such higher-order effects, for example, by using not so strong external fields.[18]

On the other hand, the one-electron reduced density $\rho(\boldsymbol{r},t)$ can be expanded as a Fourier series in the incident frequencies.[23b] The doubled-frequency component $\rho_{\mathrm{pol}}(\boldsymbol{r},2\omega)$ is obtained by the Fourier transform of $\rho_{\mathrm{pol}}(\boldsymbol{r},t)$, which approximately characterizes the second-order response of the one-electron reduced density oscillating with a frequency of 2ω. The dynamic first hyperpolarizability density (β density) is therefore defined as[23d]

$$\rho^{(2),ll}(\boldsymbol{r},\,-2\omega;\,\omega,\,\omega) = \frac{\rho_{\mathrm{pol}}(\boldsymbol{r},\,2\omega)}{2\varepsilon^l(\omega)\varepsilon^l(\omega)} \tag{7}$$

where the dynamic β density, $\rho^{(2),ll}(\boldsymbol{r},-2\omega;\omega,\omega)$, is connected with the dynamic β value by the following spatial integration

$$\beta_{lll}(-2\omega;\,\omega,\,\omega) = -\frac{1}{2!}\int r^l \rho^{(2),ll}(\boldsymbol{r},\,-2\omega;\,\omega,\,\omega)\,\mathrm{d}\boldsymbol{r} \tag{8}$$

Because the dynamic β density represents the increase and decrease of the electron density oscillating with a doubled frequency (2ω), the SHG response part in the polarization density is calculated by $\rho_{\mathrm{pol}}^{\mathrm{SHG}}(\boldsymbol{r},t) = \rho^{(2),ll}(\boldsymbol{r},-2\omega;\omega,\omega)4\varepsilon^l(\omega)\varepsilon^l(\omega)\cos 2\omega t$. Thus, the spatial contribution of field-induced electron density changes resulting in the SHG response can be investigated by plotting the map of the dynamic β density $[\rho^{(2),ll}(\boldsymbol{r},-2\omega;\omega,\omega)]$. Ye and Autschbach have also calculated the dynamic β density of several donor−acceptor-substituted conjugated molecules by using the TDDFT response theory.[28] On the other hand, in the present method, we could also treat the effect of relaxation through the QME framework,[29] though it is out of the scope in this study.

Practically, the dynamic β density is calculated by the following procedure based on the MOQME method. We first compute the SHG response part of each RDM element in the one-exciton configuration basis, $\{|i\rangle\}$, that is, $\rho_{ij}^{(2),ll}(-2\omega;\omega,\omega) = \rho_{ij}(2\omega)/2\varepsilon^l(\omega)\varepsilon^l(\omega)$, using the frequency domain RDM, $\{\rho_{ij}(2\omega)\}$. Then, we substitute these matrix elements into eq 5 and obtain the following expression for the dynamic β density

$$\begin{aligned}
&\rho^{(2),ll}(\boldsymbol{r},\,-2\omega;\,\omega,\,\omega)\\
&= \sum_{i(a\to r)=2} [(|\psi_r(\boldsymbol{r})|^2 - |\psi_a(\boldsymbol{r})|^2)\rho_{ii}^{(2),ll}(-2\omega;\,\omega,\,\omega)\\
&\quad + 2\sqrt{2}\psi_a(\boldsymbol{r})\psi_r(\boldsymbol{r})\,\mathrm{Re}[\rho_{1i}^{(2),ll}(-2\omega;\,\omega,\,\omega)]\\
&\quad + 2\sum_{j(a\to s)(>i)} \psi_r(\boldsymbol{r})\psi_s(\boldsymbol{r})\,\mathrm{Re}[\rho_{ij}^{(2),ll}(-2\omega;\,\omega,\,\omega)]\\
&\quad - 2\sum_{j(b\to r)(>i)} \psi_a(\boldsymbol{r})\psi_b(\boldsymbol{r})\,\mathrm{Re}[\rho_{ij}^{(2),ll}(-2\omega;\,\omega,\,\omega)]]
\end{aligned} \tag{9}$$

On the other hand, the system polarization oscillating with a frequency of 2ω is represented using the trace of $\rho(2\omega)$ by $P^l(2\omega) = \mathrm{tr}[\mu^l\rho(2\omega)]$, where μ is the transition dipole operator. Using eq 6, the dynamic β is therefore calculated by using the SHG response part of RDM elements $\{\rho_{ij}^{(2),ll}(-2\omega;\omega,\omega)\}$ as

$$\begin{aligned}
\beta_{lll}(-2\omega;\,\omega,\,\omega) &= \frac{1}{2!}\,\mathrm{tr}\left[\mu^l\frac{\rho(2\omega)}{2\varepsilon^l(\omega)\varepsilon^l(\omega)}\right]\\
&= \frac{1}{2!}\,\mathrm{tr}[\mu^l\rho^{(2),ll}(-2\omega;\,\omega,\,\omega)]\\
&= \frac{1}{2!}\sum_{i(\neq 1)} [\mu_{ii}^l\rho_{ii}^{(2),ll}(-2\omega;\,\omega,\,\omega)\\
&\quad + 2\mu_{1i}^l\,\mathrm{Re}[\rho_{1i}^{(2),ll}(-2\omega;\,\omega,\,\omega)]\\
&\quad + \sum_{j(\neq 1,>i)} 2\mu_{ij}^l\,\mathrm{Re}[\rho_{ij}^{(2),ll}(-2\omega;\,\omega,\,\omega)]]\\
&\equiv \sum_{i(\neq 1)} [\beta_{ii}^{lll}(-2\omega;\,\omega,\,\omega)\\
&\quad + \beta_{1i}^{lll}(-2\omega;\,\omega,\,\omega)\\
&\quad + \sum_{j(>i)} \beta_{ij}^{lll}(-2\omega;\,\omega,\,\omega)]
\end{aligned} \tag{10}$$

where $\mu_{ij}^l = -\int r^l\{d_{ij}(\boldsymbol{r}) - d_{11}(\boldsymbol{r})\delta_{ij}\}\,\mathrm{d}\boldsymbol{r}$. By evaluating each term of eq 10, that is, $\beta_{ij}^{lll}(-2\omega;\omega,\omega)$, we can analyze the contributions of excitation configurations to the total β values. Equations 9 and 10 are related to each other through eq 8. By using eqs 9 and 10, we can directly extract a specific MO pair for one-electron excitation, $|i = \psi_a \to \psi_r\rangle$, whose contribution to the dynamic β (given by the first and second terms in eq 10) is dominant in the total β value. The first term of eq 9 involves the spatial part $d_{ii}(\boldsymbol{r}) - d_{11}(\boldsymbol{r}) = |\psi_r(\boldsymbol{r})|^2 - |\psi_a(\boldsymbol{r})|^2$, which represents the difference in the densities of virtual (r) and occupied (a) MOs, while the second term involves the one-electron transition density between these MOs, $d_{1i}(\boldsymbol{r}) = \sqrt{2}\psi_a(\boldsymbol{r})\psi_r(\boldsymbol{r})$. Additionally, these densities are related to the dipole moment difference and transition dipole moment between the ground state (1) and a charge-transfer excited state (α), that is, $\Delta\mu_\alpha = \mu_{\alpha\alpha} - \mu_{11}$ and $\mu_{1\alpha}$, respectively, when the configuration $|i\rangle$ is predominant in state α. Plotting these densities as well as the orbital pair β densities defined as

dx.doi.org/10.1021/jp301213z | J. Phys. Chem. A 2012, 116, 4371−4380

$$\rho_{ii}^{(2),II}(\boldsymbol{r}, -2\omega; \omega, \omega) = \{d_{ii}(\boldsymbol{r}) - d_{11}(\boldsymbol{r})\} \times \rho_{ii}^{(2),II}(-2\omega; \omega, \omega) \quad \text{(diagonal)} \tag{11}$$

and

$$\rho_{1i}^{(2),II}(\boldsymbol{r}, -2\omega; \omega, \omega) = 2d_{1i}(\boldsymbol{r})\ \mathrm{Re}[\rho_{1i}^{(2),II}(-2\omega; \omega, \omega)] \quad \text{(off-diagonal)} \tag{12}$$

is useful for understanding the spatial contributions of a specific MO pair to the dynamic β. Note that spatial integrations of these densities give the corresponding β contributions, that is

$$\beta_{ii}^{III}(-2\omega; \omega, \omega) = -\frac{1}{2!}\int r^l \rho_{ii}^{(2),II}(\boldsymbol{r}, -2\omega; \omega, \omega)\, \mathrm{d}\boldsymbol{r} \quad \text{(diagonal)} \tag{13}$$

and

$$\beta_{1i}^{III}(-2\omega; \omega, \omega) = -\frac{1}{2!}\int r^l \rho_{1i}^{(2),II}(\boldsymbol{r}, -2\omega; \omega, \omega)\, \mathrm{d}\boldsymbol{r} \quad \text{(off-diagonal)} \tag{14}$$

Of course, there are contributions from the remaining off-diagonal matrix element $\beta_{ij}^{III}(-2\omega;\omega,\omega)$ for $i \neq 1$ and $j > i$. In such case, we have

$$\rho_{ij}^{(2),II}(\boldsymbol{r}, -2\omega; \omega, \omega) = 2d_{ij}(\boldsymbol{r})\ \mathrm{Re}[\rho_{ij}^{(2),II}(-2\omega; \omega, \omega)] \quad \text{(off-diagonal)} \tag{15}$$

and

$$\beta_{ij}^{III}(-2\omega; \omega, \omega) = -\frac{1}{2!}\int r^l \rho_{ij}^{(2),II}(\boldsymbol{r}, -2\omega; \omega, \omega) d\boldsymbol{r} \quad \text{(off-diagonal)} \tag{16}$$

The off-diagonal element of the one-electron reduced density matrix, $d_{ij}(\boldsymbol{r})$, becomes zero when two determinants $|i\rangle$ and $|j\rangle$ differ by more than two orbitals. It is noted that this off-diagonal contribution $|\beta_{ij}^{III}|$ is usually smaller than $|\beta_{ii}^{III}|$ and $|\beta_{1i}^{III}|$ within the off-resonant condition in the ground state.

Finally, we provide an explicit expression of the dynamic β density in the Mulliken approximation, which is known to be useful for semiquantitative analysis of spatial contributions of electrons to static/dynamic hyperpolarizabilities.[23] We here represent the dynamic β density by the sum of dynamic β densities partitioned into each AO p $[\rho_p^{(2),II}(\boldsymbol{r},-2\omega;\omega,\omega)]$ and each atom A $[\rho_A^{(2),II}(\boldsymbol{r},-2\omega;\omega,\omega)]$[23a]

$$\begin{aligned}\rho^{(2),II}(\boldsymbol{r}, -2\omega; \omega, \omega) &= \sum_p \rho_p^{(2),II}(\boldsymbol{r}, -2\omega; \omega, \omega) \\ &= \sum_A \rho_A^{(2),II}(\boldsymbol{r}, -2\omega; \omega, \omega)\end{aligned} \tag{17a}$$

where the atomic dynamic β density $[\rho_A^{(2),II}(\boldsymbol{r},-2\omega;\omega,\omega)]$ on atom A is defined by

$$\rho_A^{(2),II}(\boldsymbol{r}, -2\omega; \omega, \omega) = \sum_{p\in A} \rho_p^{(2),II}(\boldsymbol{r}, -2\omega; \omega, \omega) \tag{17b}$$

The spatial integration of eq 17a gives

$$\begin{aligned}\int \rho^{(2),II}(\boldsymbol{r}, -2\omega; \omega, \omega)\, \mathrm{d}\boldsymbol{r} &= \sum_A \int \rho_A^{(2),II}(\boldsymbol{r}, -2\omega; \omega, \omega)\, \mathrm{d}\boldsymbol{r} \\ &= 0\end{aligned} \tag{18a}$$

On the other hand, the following equation is obtained by introducing the linear combination of atomic orbital (LCAO) expansion for MOs into eq 9

$$\begin{aligned}\int \rho^{(2),II}(\boldsymbol{r}, -2\omega; \omega, \omega)\, \mathrm{d}\boldsymbol{r} &= \sum_{pq}\sum_{i(a\to r)=2} [(c_r^p c_r^q - c_a^p c_a^q)\rho_{ii}^{(2),II}(-2\omega; \omega, \omega) \\ &\quad + 2\sqrt{2}\, c_a^p c_r^q\ \mathrm{Re}[\rho_{1i}^{(2),II}(-2\omega; \omega, \omega)] \\ &\quad + 2\sum_{j(a\to s)(>i)} c_r^p c_s^q\ \mathrm{Re}[\rho_{ij}^{(2),II}(-2\omega; \omega, \omega)] \\ &\quad - 2\sum_{j(b\to r)(>i)} c_a^p c_b^q\ \mathrm{Re}[\rho_{ij}^{(2),II}(-2\omega; \omega, \omega)]]S_{qp} \\ &\equiv \sum_{pq} D_{pq}^{(2)}(-2\omega; \omega, \omega)S_{qp} \\ &= \sum_p [\boldsymbol{D}^{(2)}(-2\omega; \omega, \omega)\boldsymbol{S}]_{pp} \\ &= \sum_A q_A^{(2),II}(-2\omega; \omega, \omega) = 0\end{aligned} \tag{18b}$$

Here, c_r^p, c_r^q, ... are the LCAO coefficients, $\boldsymbol{S}$ is the overlap matrix, $\boldsymbol{D}^{(2)}(-2\omega;\omega,\omega)$ is the second-order response density matrix in the AO basis, and $q_A^{(2),II}(-2\omega;\omega,\omega)$ is given by

$$q_A^{(2),II}(-2\omega; \omega, \omega) = \sum_{p\in A} [\boldsymbol{D}^{(2)}(-2\omega; \omega, \omega)\boldsymbol{S}]_{pp} \tag{18c}$$

In comparison of eq 18a with eq 18b, we can obtain the following expression in the Mulliken approximation[23a]

$$\rho_A^{(2),II}(\boldsymbol{r}, -2\omega; \omega, \omega) \approx q_A^{(2),II}(-2\omega; \omega, \omega)\delta(\boldsymbol{r} - \boldsymbol{r}_A) \tag{19}$$

From eqs 8 and 19, the dynamic β in the Mulliken approximation $[\beta_{III}^{\mathrm{Mulliken}}(-2\omega;\omega,\omega)]$ can be obtained by

$$\begin{aligned}\beta_{III}(-2\omega; \omega, \omega) &= -\frac{1}{2!}\sum_A \int r^l \rho_A^{(2),II}(\boldsymbol{r}, -2\omega; \omega, \omega)\, \mathrm{d}\boldsymbol{r} \\ &\approx -\frac{1}{2!}\sum_A \int r^l q_A^{(2),II}(-2\omega; \omega, \omega) \\ &\quad \times \delta(\boldsymbol{r} - \boldsymbol{r}_A)\, \mathrm{d}\boldsymbol{r} \\ &= -\frac{1}{2!}\sum_A r_A^l q_A^{(2),II}(-2\omega; \omega, \omega) \\ &\equiv \beta_{III}^{\mathrm{Mulliken}}(-2\omega; \omega, \omega)\end{aligned} \tag{20}$$

Here, $q_A^{(2),II}(-2\omega;\omega,\omega)$ indicates the Mulliken dynamic β density, which is a dynamic extension of the Mulliken static β density.[23a]

dx.doi.org/10.1021/jp301213z | J. Phys. Chem. A 2012, 116, 4371−4380

3. COMPUTATIONAL DETAILS

We examine donor (NH_2)- and/or acceptor (NO_2)-substituted benzenes (systems **1**−**3**) shown in Figure 1. Each molecular

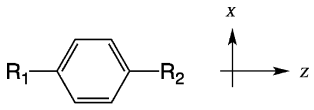

1 $R_1 = H, R_2 = NH_2$
2 $R_1 = NO_2, R_2 = H$
3 $R_1 = NO_2, R_2 = NH_2$

Figure 1. Calculated molecular systems as well as the coordinate axis.

geometry is optimized at the B3LYP/6-31G** level of approximation under the constraint of C_{2v} symmetry. In the CIS calculations, we obtain all of the excited states by taking account of the valence π-orbitals as the active space using the 6-31G** basis set (see Figure 2). We also calculate the unrelaxed permanent dipole moment[30] of each electronic state using the CIS wave function. All of the ab initio calculations were performed using the Gaussian 03 program package.[31]

On the basis of the electronic transition properties, we numerically solve the equation of motion of exciton RDM, eqs 2 and 3, by the sixth-order Runge−Kutta method in the presence of two cw laser fields. Both of the fields oscillate along the longitudinal z-axis with the same frequency of ω = 3000 cm^{-1}, which is in far off-resonant condition. The power of the fields is set to 100 MW/cm^2, which is strong enough to observe the longitudinal SHG signal, $\beta_{zzz}(-2\omega;\omega,\omega)$. The relaxation factors Γ appearing in eqs 2 and 3 are neglected in this study because the effect of relaxation has been already discussed in our previous study,[29] while we set the additional damping factor from the excited state to the ground state, $\Gamma_{\alpha 1} = 0.01\omega_\alpha$. The time evolution of exciton RDM is calculated up to 3000 optical cycles. Each optical cycle is divided into 1000 numerical calculation steps. We then employ the results of $P^z(t)$ and $\{\rho_{\alpha\beta}(t)\}$ of the last 2000 optical cycles for the numerical Fourier transformation to obtain $\beta_{zzz}(-2\omega;\omega,\omega)$ $(\equiv\beta(-2\omega;\omega,\omega))$ and $\{\rho_{ij}^{(2),zz}(-2\omega;\omega,\omega)\}$ $(\equiv \{\rho_{ij}^{(2)}(-2\omega;\omega,\omega)\})$. Hereafter, we drop the sub- and superscripts "z" representing the longitudinal z-axis component for the β and its densities. For comparison, the SOS dynamic β is also calculated by using the same excitation energies and transition dipole moment matrix as that used in the MOQME calculations.

4. RESULTS AND DISCUSSION

All of the active MOs of these systems are shown in Figure 2. For system **1**, HOMO and LUMO+1 have spatial distributions on the donor (NH_2) region, while for system **2**, HOMO−1 and LUMO+1 do on the acceptor (NO_2) region. In the case of system **3**, HOMO and LUMO have distributions on both the donor (NH_2) and acceptor (NO_2) regions. In Table 1, we summarize the electronic excitation energies (E_α) and transition properties (transition dipole moment $\mu_{1\alpha}^z$ and dipole moment difference $\Delta\mu_\alpha^z = \mu_{\alpha\alpha}^z - \mu_{11}^z$) between the ground state and the lowest-lying excited state α with a nonzero $\mu_{1\alpha}^z$ value (the lowest-lying excited state with A_1 symmetry). For systems **1** and **2**, the excited state is described by HOMO−1 → LUMO and HOMO → LUMO+1 transitions, while for system **3**, it is characterized by a HOMO → LUMO transition. The excitation energy decreases in the order **1** > **2** > **3**. The charge-transfer character of this excited state, that is, the amplitude of $\Delta\mu_\alpha^z$, as well as the amplitude of the transition dipole moment, $|\mu_{1\alpha}^z|$, turns out to increase in the order of **1**(NH_2) < **2**(NO_2) < **3**(NO_2/NH_2), which agrees with the order of strength of push/pull effects of these substituent groups.

Table 1. Calculated Excitation Energy, E_α, Transition Dipole Moment, $\mu_{1\alpha}^z$, and Dipole Moment Difference, $\Delta\mu_\alpha^z$, for the Lowest-Lying CT State α Characterized by Non-Zero $\mu_{1\alpha}^z$ Value for Systems 1−3

	1	2	3
state number α	3	3	2
E_α [eV]	6.87	6.43	5.87
$\lvert\mu_{1\alpha}^z\rvert$ [D]	1.70	3.21	5.51
$\Delta\mu_\alpha^z$ [D]	0.88	3.84	5.91
CI coefficients[a]	H → L+1 0.792 H−1 → L −0.600	H → L+1 0.4295 H−1 → L 0.885	H → L 0.933

[a]H and L denote the HOMO and LUMO, respectively.

In Table 2, we compare the dynamic β values calculated from the MOQME method with those from the SOS method. The β amplitude increases in the order **1** < **2** < **3**. The numerical β values using the MOQME method are shown to be in agreement with the SOS results within 1% relative numerical error. As was reported in the previous study, the present numerical method is shown to achieve sufficient accuracy for the dynamic β, if we set an appropriate calculation condition.[18] Applying the two-state approximation, the SOS dynamic β is expressed as

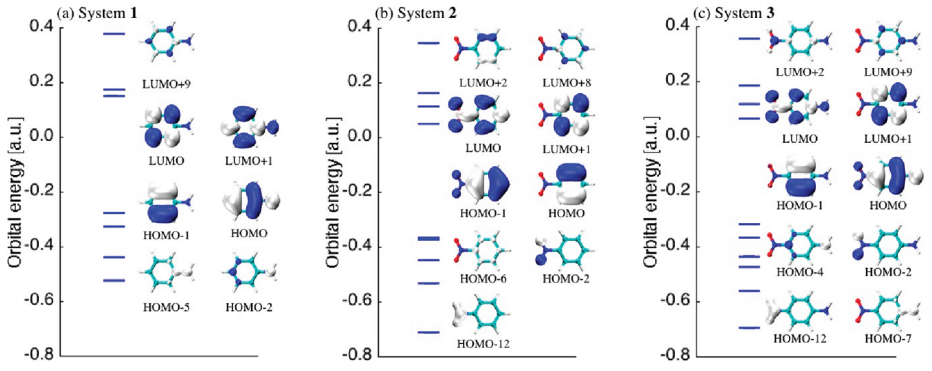

Figure 2. Isosurface maps [white (+) and blue (−) contours with an amplitude of 0.01 au] of active MOs of systems **1** (a), **2** (b), and **3** (c) together with their orbital energy diagrams calculated at the HF/6-31G** level of approximation.

dx.doi.org/10.1021/jp301213z | J. Phys. Chem. A 2012, 116, 4371−4380

Table 2. Comparison of $\beta(-2\omega;\omega,\omega)$ (au) (ω = 3000 cm^{-1}) for Systems 1−3 Calculated by the MOQME and SOS Methods

method	1	2	3
MOQME	224.6	341.1	1056.0
SOS	224.3	340.8	1054.8
SOS (two states)	7.4	132.2	717.0

$$\beta_{zzz}^{\text{two-state}}(-2\omega;\,\omega,\,\omega) = \frac{3(\mu_{1\alpha}^{z})^2 \Delta\mu_{\alpha}^{z} E_{\alpha}^{2}}{(E_{\alpha}^{2} - \hbar\omega^{2})(E_{\alpha}^{2} - 4\hbar\omega^{2})} \quad (21)$$

We also show the results of the SOS within the two-state approximation in Table 2. The two-state β amplitude increases in the order **1** < **2** < **3**, which agrees with the order of total β values. However, the two-state approximation is shown to provide only 3, 39, and 68% of the total β values of systems **1**, **2**, and **3**, respectively. These results indicate that there are important higher-lying excited states contributing to β except for the lowest-lying CT state, in particular, for systems **1** and **2**.

Figure 3 shows the isosurface maps of polarization density $\rho_{\text{pol}}(\boldsymbol{r},t)$ for the 3000th optical cycle at times $\omega t = 0 + 2n\pi$, $\pi/2 + 2n\pi$, $\pi + 2n\pi$, $3\pi/2 + 2n\pi$, and $2\pi + 2n\pi$ calculated from eq 6 (see also the movies in the Supporting Information) together with the maps of polarizability density $\rho^{(1),I}(\boldsymbol{r},-\omega;\omega)$ $[\equiv\rho^{(1)}(\boldsymbol{r},-\omega;\omega)] = \rho_{\text{pol}}(\boldsymbol{r},\omega)/2\varepsilon^{I}(\omega)$. Yellow and blue meshes represent the increase and decrease regions of charge densities, respectively. For all systems, positive and negative $\rho_{\text{pol}}(\boldsymbol{r},t)$ are found to be well-separated on both sides of the molecule, except for those on the N atom of the NO_2 group. When the direction of the external field coincides with the positive direction of the coordinate axis, the electronic polarization vector is observed to be also in the positive direction, and vice versa. The dynamic behavior of $\rho_{\text{pol}}(\boldsymbol{r},t)$ is well-characterized by $\rho^{(1)}(\boldsymbol{r},-\omega;\omega)$, which corresponds to the Fourier component with a frequency ω of $\rho_{\text{pol}}(\boldsymbol{r},t)$. Therefore, the linear response part (Fourier component with ω) of the charge density is shown to be dominant in the total response of the charge density. For systems **1** and **2**, virtual charge transfer is shown to occur between the benzene ring and substitution group. On the other hand, for system **3**, the charge transfer is found to occur in the entire region of the molecule involving the donor and acceptor groups. Apparently, the amount of the charge transfer and its distance in system **3** are the largest among the three systems.

Figure 4 shows the isosurface maps of the dynamic β density $[\rho^{(2)}(\boldsymbol{r},-2\omega;\omega,\omega)]$ (see also the movies for the SHG response density $\rho^{(2)}(\boldsymbol{r},-2\omega;\omega,\omega)\cos 2\omega t$ in the Supporting Information). Yellow and blue meshes represent the positive and negative $\rho^{(2)}(\boldsymbol{r},-2\omega;\omega,\omega)$, respectively. The relationship between β and $\rho^{(2)}(\boldsymbol{r},-2\omega;\omega,\omega)$ is explained by considering a simple example, a pair of localized β densities with positive and negative values. The sign of the contribution to β is positive when the direction from the positive to negative β density coincides with the positive direction of the coordinate axis. The sign becomes negative in the opposite case. Moreover, the

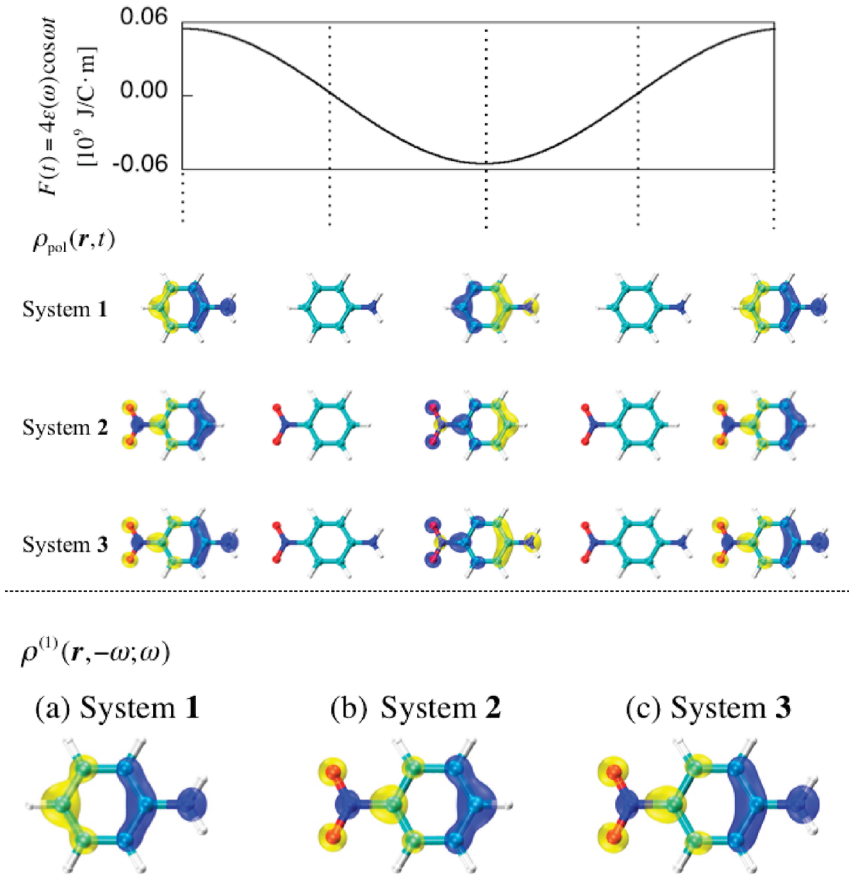

Figure 3. External electric field $F(t)$ and isosurface maps of the polarization density, $\rho_{\text{pol}}(\boldsymbol{r},t)$ at $\omega t = 0 + 2n\pi$, $\pi/2 + 2n\pi$, $\pi + 2n\pi$, $3\pi/2 + 2n\pi$, and $2\pi + 2n\pi$ for the 3000th optical cycle. The polarizability density $\rho^{(1)}(\boldsymbol{r},-\omega;\omega)$ is also shown. Yellow and blue meshes represent the positive and negative contributions, respectively, with the contour values of $\pm 10^{-5}$ au for $\rho_{\text{pol}}(\boldsymbol{r},t)$ and ± 0.1 au for $\rho^{(1)}(\boldsymbol{r},-\omega;\omega)$, respectively.

dx.doi.org/10.1021/jp301213z | J. Phys. Chem. A 2012, 116, 4371−4380

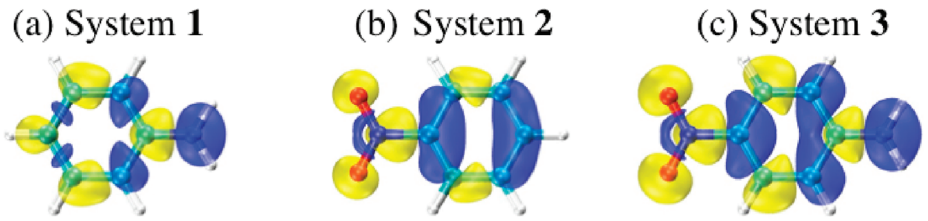

Figure 4. Isosurface maps of the dynamic β density $[\rho^{(2)}(r,-2\omega;\omega,\omega)]$. Yellow and blue meshes represent the positive and negative contributions, respectively, with the contour values of ±0.5 au.

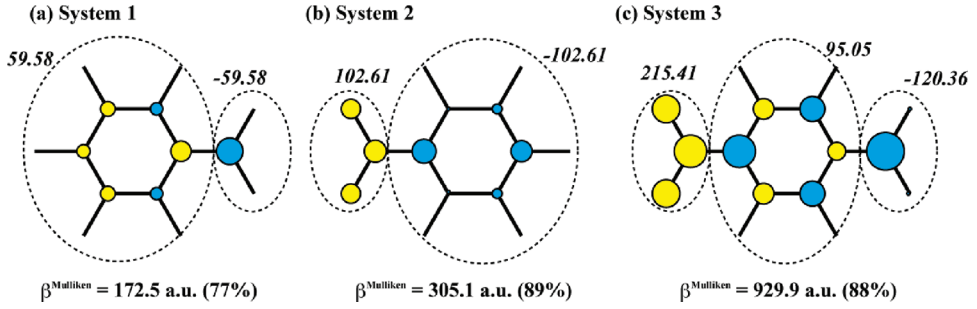

Figure 5. Maps of the Mulliken dynamic β density $[\rho_A^{(2)}(-2\omega;\omega,\omega)]$. Areas of yellow and blue circles represent the amplitudes of positive and negative contributions, respectively. Values in italic characters represent the sum of the contributions $q_A^{(2)}(-2\omega;\omega,\omega)$ in au for the donor, benzene ring, and acceptor regions. The $\beta^{\text{Mulliken}}(-2\omega;\omega,\omega)$ values calculated by eq 18c and their percentages with respect to the original dynamic β values are also shown.

magnitude of the contribution associated with this pair of β densities is proportional to the distance between them. From the definitions in eqs 4 and 7, the changes in the electron density oscillating with the doubled frequency (2ω) are involved in the total response $\rho_{\text{pol}}(r,t)$. However, spatial distributions and nodes of $\rho^{(1)}(r,-\omega;\omega)$ (see Figure 3) and $\rho^{(2)}(r,-2\omega;\omega,\omega)$ are found to appear in the mutually different regions. Such differences in the spatial distributions and nodes of the densities originate in the difference of virtual transition processes between the linear and second-order response phenomena. For system **1**, positive and negative β densities appear primarily on the benzene ring and donor regions, respectively, the feature of which indicates a charge transfer between the donor (NH_2) and the benzene ring. On the other hand, positive and negative β densities of system **2** appear in the acceptor (NO_2) and ring regions, respectively, indicating a charge transfer between the benzene ring and the acceptor group. Although the topology of positive and negative β density distributions of system **3** agrees well with that of the sum of β densities of systems **1** and **2**, the density amplitudes of system **3** are found to be larger than those of systems **1** and **2**. This indicates the nonadditivity of β among these substituted systems. For system **3**, large positive and negative β densities are observed on the donor and acceptor regions, respectively, as well as on the benzene ring, where positive and negative densities alternately appear, and thus, their contributions to β cancel with each other. In order to semiquantitatively confirm such nonadditivity of β, we perform the Mulliken population analysis for the dynamic β. Figure 5 shows the Mulliken dynamic β density calculated by eq 18c. The approximate dynamic β values in the Mulliken approximation are found to reproduce ∼80−90% of the β values calculated by eq 10. Apparently, the amplitudes of positive and negative β densities in the donor, acceptor, and central ring regions of system **3** are enhanced as compared to those in the corresponding regions of systems **1** and **2**, that is, the donor (−59.58), benzene (−43.03), and acceptor (102.61) for system **1** + **2** versus the donor (−120.36), benzene (−95.05), and acceptor (215.41) for system **3**. As a result, a cooperative effect of the donor and acceptor groups through the central conjugation ring on the charge transfer between the both-end groups is shown to be induced in such a donor−acceptor disubstituted π-conjugated system, which causes a nonlinear enhancement of the longitudinal β amplitude.

Table 3 summarizes the main contributions of $\beta_{ii}(-2\omega;\omega,\omega)$ and $\beta_{1i}(-2\omega;\omega,\omega)$ defined by eq 10. The dynamic β of systems **1**, **2**, and **3** are mainly described by the HOMO−LUMO+1 pair, HOMO−1−LUMO pair, and HOMO−LUMO pair contributions, respectively. The contribution of the HOMO−LUMO+1 pair for system **1** is found to reach 77% of the total β value (224.6 au). For system **2**, the contribution of the HOMO−1−LUMO pair is shown to exceed the total β value (341.1 au) by 152%. However, we found that there are several pairs negatively contributing to β, for example, −64 au (the HOMO−1−LUMO+2 pair). The main contribution of the HOMO−LUMO pair in system **3** is also found to exceed the total β value (1056.0 au) by 127%. Again, we observe negative contribution of the HOMO−1−LUMO+1 pair (−108 au). From Table 3, the amplitude of off-diagonal $\beta_{1i}(-2\omega;\omega,\omega)$ is

Table 3. Main Contributions of $\beta_{ii}(-2\omega;\omega,\omega)$ and $\beta_{1i}(-2\omega;\omega,\omega)$ Together with the Sum of These Contributions (au) for Systems 1−3

system	$\|i = \psi_a \rightarrow \psi_r\rangle$	$\beta_{ii}(-2\omega;\omega,\omega)$	$\beta_{1i}(-2\omega;\omega,\omega)$	sum
1	$\|\psi_H \rightarrow \psi_{L+1}\rangle$	48	125	173
	$\|\psi_{H-1} \rightarrow \psi_L\rangle$	5	10	15
2	$\|\psi_{H-1} \rightarrow \psi_L\rangle$	195	323	518
	$\|\psi_{H-1} \rightarrow \psi_{L+2}\rangle$	2	−66	−64
3	$\|\psi_H \rightarrow \psi_L\rangle$	516	826	1342
	$\|\psi_{H-1} \rightarrow \psi_{L+1}\rangle$	10	−118	−108

dx.doi.org/10.1021/jp301213z | J. Phys. Chem. A 2012, 116, 4371−4380

shown to be larger than that of diagonal $\beta_{ii}(-2\omega;\omega,\omega)$ for the configurations $\{|i = \psi_a \rightarrow \psi_r\rangle\}$. This can be attributed to (i) the prefactor of 2 appearing in eq 12 so as to sum up the off-diagonal parts twice and (ii) the small value of $|\rho_{ij}^{(2),II}(-2\omega;\omega,\omega)|$ compared to the off-diagonal $|\rho_{ij}^{(2),II}(-2\omega;\omega,\omega)|$ in the off-resonant condition. The diagonal $|\rho_{ij}^{(2),II}(-2\omega;\omega,\omega)|$ is expected to become large when large excited-state populations are observed by the irradiation of the (near-)resonant field, while the present calculation is performed in the off-resonant condition. In this relation, analysis of frequency dispersion of $\{\rho_{ij}^{(2),II}(-2\omega;\omega,\omega)\}$ and dynamic β is considered to be an interesting subject to be studied by the MOQME method. Table 4 shows the contributions of the other off-diagonal elements, that is, $\beta_{ij}(-2\omega;\omega,\omega)$. It is found that the amplitudes of their contributions are more than 10% of the largest $\beta_{ii}(-2\omega;\omega,\omega)$ and $\beta_{li}(-2\omega;\omega,\omega)$ contributions and are comparable to the second largest one. Nevertheless, semiquantitative analysis of the dominant spatial contributions of the dynamic β is found to be provided based on the pairs giving the largest contributions.

Table 4. Top Two Contributions of the Off-Diagonal $\beta_{ij}(-2\omega;\omega,\omega)$ (au) for Systems 1−3

system	$\|i = \psi_a \rightarrow \psi_r\rangle$	$\|j = \psi_b \rightarrow \psi_s\rangle$	$\beta_{ij}(-2\omega;\omega,\omega)$
1	$\|\psi_{H-2} \rightarrow \psi_{L+1}\rangle$	$\|\psi_H \rightarrow \psi_{L+1}\rangle$	23
	$\|\psi_H \rightarrow \psi_{L+1}\rangle$	$\|\psi_H \rightarrow \psi_{L+9}\rangle$	−7
2	$\|\psi_{H-1} \rightarrow \psi_L\rangle$	$\|\psi_{H-1} \rightarrow \psi_{L+2}\rangle$	−86
	$\|\psi_{H-6} \rightarrow \psi_L\rangle$	$\|\psi_{H-1} \rightarrow \psi_L\rangle$	−80
3	$\|\psi_H \rightarrow \psi_L\rangle$	$\|\psi_H \rightarrow \psi_{L+2}\rangle$	−140
	$\|\psi_{H-4} \rightarrow \psi_L\rangle$	$\|\psi_H \rightarrow \psi_L\rangle$	−75

Figure 6 shows the isosurface maps of the one-electron reduced density matrices $d_{ii}(\boldsymbol{r}) - d_{11}(\boldsymbol{r}) = |\psi_r(\boldsymbol{r})|^2 - |\psi_a(\boldsymbol{r})|^2$ and $d_{li}(\boldsymbol{r}) = \sqrt{2}\psi_a(\boldsymbol{r})\psi_r(\boldsymbol{r})$ as well as the diagonal and off-diagonal pair β densities, $\rho_{ii}^{(2),II}(\boldsymbol{r},-2\omega;\omega,\omega)$ and $\rho_{li}^{(2),II}(\boldsymbol{r},-2\omega;\omega,\omega)$, defined by eqs 11 and 12 for the configuration $|i = \psi_a \rightarrow \psi_r\rangle$ giving the largest contribution to the total β. The density $|\psi_{L+1}(\boldsymbol{r})|^2 - |\psi_H(\boldsymbol{r})|^2$ of system **1** is the difference in the distributions between LUMO+1 and HOMO (see Figure 2a), where large density amplitudes appear around the donor region. On the other hand, $\sqrt{2}\psi_H(\boldsymbol{r})\psi_{L+1}(\boldsymbol{r})$ is the one-electron transition density between the HOMO and LUMO+1, where negative and positive densities are observed around the donor region, that is, the C−N region, and the opposite side C atom in the benzene ring, respectively. As a result, both $\rho_{ii}^{(2),II}(\boldsymbol{r},-2\omega;\omega,\omega)$ and $\rho_{li}^{(2),II}(\boldsymbol{r},-2\omega;\omega,\omega)$ exhibit the positive and negative contributions on the left- and right-hand-side regions, leading to the positive β value. For system **2**, the HOMO−1 and LUMO as well as $|\psi_L(\boldsymbol{r})|^2 - |\psi_{H-1}(\boldsymbol{r})|^2$ and $\sqrt{2}\psi_{H-1}(\boldsymbol{r})\psi_L(\boldsymbol{r})$ are distributed on both the benzene ring and acceptor regions, where positive and negative densities of $\rho_{ii}^{(2),II}(\boldsymbol{r},-2\omega;\omega,\omega)$ and $\rho_{li}^{(2),II}(\boldsymbol{r},-2\omega;\omega,\omega)$ appear around the acceptor and ring regions, respectively. For system **3**, both the $|\psi_L(\boldsymbol{r})|^2 - |\psi_H(\boldsymbol{r})|^2$ and $\sqrt{2}\psi_H(\boldsymbol{r})\psi_L(\boldsymbol{r})$ are shown to have distributions on the donor (positive), benzene ring (positive/negative), and acceptor (negative) regions, which indicate the charge transfer between the donor and acceptor groups through the benzene ring. The maps of the β densities of these MO pairs are shown to be very similar to those of the total β densities (see Figures 4 and 5) in their shapes and amplitudes. Thus, these MO pairs are found to play a crucial role in the SHG response of the electron density with respect to the applied dynamic electric field.

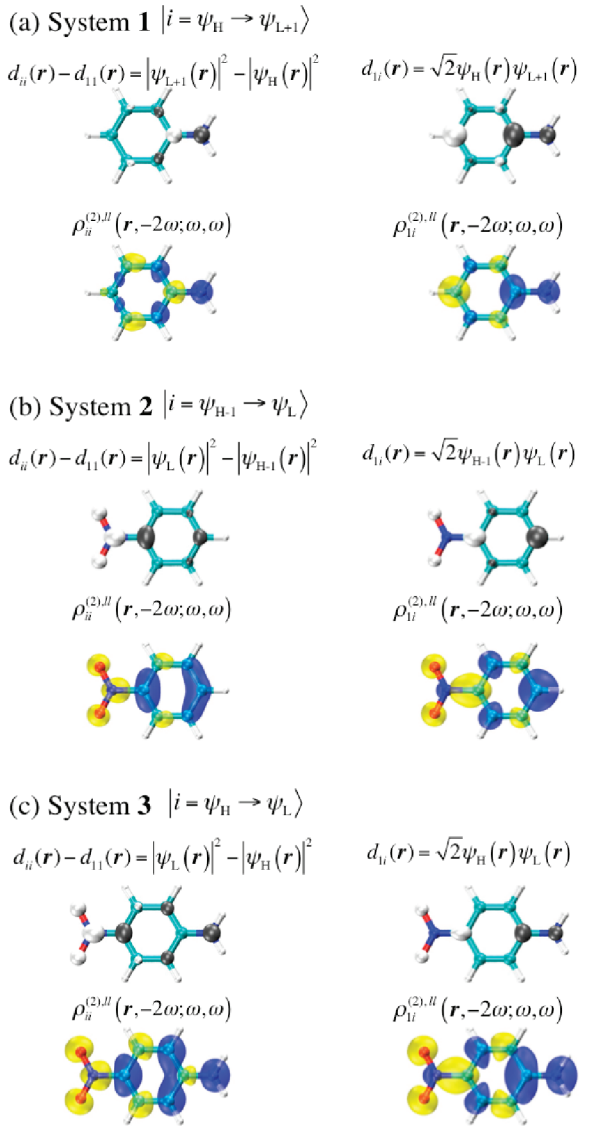

Figure 6. Isosurface maps of $d_{ii}(\boldsymbol{r}) - d_{11}(\boldsymbol{r}) = |\psi_r(\boldsymbol{r})|^2 - |\psi_a(\boldsymbol{r})|^2$ and $d_{li}(\boldsymbol{r}) = \sqrt{2}\psi_a(\boldsymbol{r})\psi_r(\boldsymbol{r})$ (white and black surfaces show the isosurfaces of ±0.04 au) as well as $\rho_{ii}^{(2)}(\boldsymbol{r},-2\omega;\omega,\omega)$ and $\rho_{li}^{(2)}(\boldsymbol{r},-2\omega;\omega,\omega)$ defined by eqs 11 and 12 (yellow and blue surfaces show the isosurfaces of ±0.5 au) for configuration $|i = \psi_a \rightarrow \psi_r\rangle$, giving the largest contribution to the total β.

From these analyses, the partition of the dynamic β and its density into the MO contributions reveals the essential MOs that enhance/reduce the dynamic β. It is found for these systems that the β value is primarily described from the excitations between the frontier MOs. In order to enhance the β amplitude, both $|\psi_r(\boldsymbol{r})|^2 - |\psi_a(\boldsymbol{r})|^2$ and $\sqrt{2}\psi_a(\boldsymbol{r})\psi_r(\boldsymbol{r})$ are required to have large positive and negative regions with a long interval. Therefore, for the donor/acceptor disubstituted systems, not only the actual charge separation in the donor−acceptor region between the ground and the excited states described by the HOMO−LUMO excitation but also the overlap between the HOMO and LUMO is found to be important to enhance the β amplitude. The present MOQME method is therefore expected to be a powerful tool for

dx.doi.org/10.1021/jp301213z | J. Phys. Chem. A 2012, 116, 4371−4380

understanding the dynamic behavior in the second-order NLO responses and for the MO-based control of the dynamic β.

5. SUMMARY AND PROSPECTS

We have developed a novel method for calculation and analysis of dynamic β based on the MOQME method. This presents a partitioning scheme of dynamic β and its density into the contributions of specific MO pairs, which is useful for revealing the crucial MO contributions and their spatial contributions to the total dynamic β. As examples, we have applied the present method to the evaluation of the dynamic β of donor (NH_2)-/acceptor (NO_2)-substituted benzenes. The dynamic β density analysis for these systems illuminates the spatial charge transfer between donor/acceptor groups and the benzene ring for monosubstituted benzenes and between donor and acceptor groups via the benzene ring for disubstituted benzenes. These charge transfers are found to be primarily described by the frontier MO pairs, where not only the one-electron dipole moment difference density but also the one-electron transition density between the MO pairs is important to enhance the dynamic β amplitude.

In the present study, we have proposed the MOQME scheme for dynamic β based on the CIS excited-state calculations. On the other hand, as is well-known, the electron correlation effects are essential for describing the dynamic β of several π-conjugated molecules such as polycyclic aromatic hydrocarbons (PAHs). Therefore, we need to improve a method for calculation of excited states in order to obtain the quantitative description of NLO properties of these systems. In this regard, the TDDFT method is considered to be the most easily accessible method giving semiquantitative β values. Indeed, we have already proposed such an approach, referred to as DFTQME, for the calculation of the dynamic α,[22] though the reliability of the TDDFT results is found to strongly depend on the choice of the exchange−correlation functional. Although the exchange−correlation functional dependence of DFT static and dynamic β values has been investigated extensively,[32,33] detailed analysis in relation to the electron dynamics, for example, the second-order optical response of the electron density, has not been performed yet. The extension of the present MOQME to the DFTQME method for evaluating dynamic β of extended π-conjugated systems including PAHs with significant electron correlations will be a challenging theme at the next stage.

■ ASSOCIATED CONTENT

Supporting Information

Movie sequences of the polarization density $\rho_{pol}(r,t)$ of systems **1**−**3** (jp301213z_si_002.qt, jp301213z_si_003.qt, jp301213z_si_004.qt) as well as those of the SHG response density $\rho^{(2)}(r,-2\omega;\omega,\omega)\cos 2\omega t$ of systems **1**−**3** (jp301213z_si_005.qt, jp301213z_si_006.qt, jp301213z_si_007.qt). This material is available free of charge via the Internet at http://pubs.acs.org.

■ AUTHOR INFORMATION

Corresponding Author

*E-mail: rkishi@cheng.es.osaka-u.ac.jp (R.K.); mnaka@cheng.es.osaka-u.ac.jp (M.N.).

Notes

The authors declare no competing financial interest.

■ ACKNOWLEDGMENTS

This work is supported by a Grant-in-Aid for Scientific Research (No. 21350011) from the Japan Society for the Promotion of Science (JSPS), the global COE (center of excellence) program "Global Education and Research Center for Bio-Environmental Chemistry" of Osaka University, and Toyota Physical & Chemical Research Institute Scholars. Theoretical calculations for the QME dynamics were partly performed using the Research Center for Computational Science, Okazaki, Japan.

■ REFERENCES

(1) (a) Prasad, P. N.; Williams, D. J. *Introduction to Nonlinear Optical Effects in Molecules and Polymers*; Wiley: New York, 1990. (b) Bosshard, Ch.; Sutter, K.; Prêtre, Ph.; Hulliger, J.; Flörsheimer, M.; Kaatz, P.; Günter, P. Organic Nonlinear Optical Materials., In *Advances in Nonlinear Optics*; Garito, A. F., Kajzar, F., Eds.; Gordon & Breach Science Pub.: Basel, Switzerland, 1995. (c) Champagne, B.; Kirtman, B.; In *Handbook of Advanced Electronic and Photonic Materials and Devices*; Nalwa, H. S., Ed.; Academic Press: New York, 2001; Vol. 9, Chapter 2, p 63. (d) Papadopoulos, M. G., Sadlej, A. J., Leszczynski, J., Eds.; *Non-Linear Optical Properties of Matter — From Molecules to Condensed Phases*; Springer: Dordrecht, The Netherlands, 2006.

(2) (a) Datta, A.; Pati, S. K. *Chem. Soc. Rev.* **2006**, *35*, 1305. (b) Kanis, D. R.; Ratner, M. A.; Marks, T. J. *Chem. Rev.* **1994**, *94*, 195. (c) Kirtman, B.; Champagne, B. *Int. Rev. Phys. Chem.* **1997**, *16*, 389.

(3) (a) Shelton, D. P. *J. Chem. Phys.* **2001**, *114*, 9938. (b) Shelton, D. P. *J. Chem. Phys.* **2002**, *117*, 9374. (c) Shelton, D. P. *J. Chem. Phys.* **2004**, *121*, 3349.

(4) (a) Głaz, W.; Bancewicz, T.; Godet, J.-L.; Maroulis, G.; Haskopoulos, A. *Phys. Rev. A* **2006**, *73*, 042708. (b) Bancewicz, T.; Maroulis, G. *Phys. Rev. A* **2009**, *79*, 042704. (c) Godet, J.-L.; Bancewicz, T.; Głaz, W.; Maroulis, G.; Haskopoulos. *J. Chem. Phys.* **2009**, *131*, 204305.

(5) (a) Orr, B. J.; Ward, J. F. *Mol. Phys.* **1971**, *20*, 513. (b) Bishop, D. M. *J. Chem. Phys.* **1994**, *100*, 6535.

(6) (a) Sekino, H.; Bartlett, R. J. *J. Chem. Phys.* **1986**, *85*, 976. (b) Karna, S. P.; Dupuis, M. *J. Comput. Chem.* **1991**, *12*, 487.

(7) (a) v. Gisbergen, S. J. A.; Snijders, J.; Baerends, E. J. *Phys. Rev. Lett.* **1997**, *78*, 3097. (b) v. Gisbergen, S. J. A.; Snijders, J.; Baerends, E. J. *J. Chem. Phys.* **1998**, *109*, 10644. (c) v. Gisbergen, S. J. A.; Snijders, J.; Baerends, E. J. *J. Chem. Phys.* **1999**, *111*, 6652(E). (d) v. Gisbergen, S. J. A.; Snijders, J.; Baerends, E. J. *J. Chem. Phys.* **1998**, *109*, 10657.

(8) (a) Christiansen, O.; Hättig, C.; Gauss, J. *J. Chem. Phys.* **1998**, *109*, 4745. (b) Larsen, H.; Olsen, J.; Hättig, C.; Jørgensen, P.; Christiansen, O.; Gauss, J. *J. Chem. Phys.* **1999**, *111*, 1917.

(9) (a) Kobayashi, T.; Sasagane, K.; Aiga, F.; Yamaguchi, K. *J. Chem. Phys.* **1999**, *111*, 842. (b) Aiga, F.; Tada, T.; Yoshimura, R. *J. Chem. Phys.* **1999**, *111*, 2878.

(10) Sugino, O.; Miyamoto, Y. *Phys. Rev. B* **1999**, *59*, 2579.

(11) Craig, C. F.; Duncan, W. R.; Prezhdo, O. V. *Phys. Rev. Lett.* **2005**, *95*, 163001.

(12) Yabana, K.; Bertsch, G. F. *Phys. Rev. B* **1996**, *54*, 4484.

(13) Baer, R. *Phys. Rev. A* **2000**, *62*, 063810.

(14) Yam, C. Y.; Yokojima, S.; Chen, G. H. *J. Chem. Phys.* **2003**, *119*, 8794.

(15) Sun, J.; Song, J.; Zhao, Y.; Liang, W. Z. *J. Chem. Phys.* **2007**, *127*, 234107.

(16) Guo, Z.; Liang, W. Z.; Zhao, Y.; Chen, G. H. *J. Phys. Chem. C* **2008**, *112*, 16655.

(17) Akama, T.; Nakai, H. *J. Chem. Phys.* **2010**, *132*, 054104.

(18) (a) Nakano, M.; Yamaguchi, K. *Phys. Rev. A* **1994**, *50*, 2989. (b) Nakano, M.; Yamaguchi, K.; Matsuzaki, Y.; Tanaka, K.; Yamabe, T. *J. Chem. Phys.* **1995**, *102*, 2986. (c) Nakano, M.; Yamaguchi, K.; Matsuzaki, Y.; Tanaka, K.; Yamabe, T. *J. Chem. Phys.* **1995**, *102*, 2996.

(19) Wang, F.; Yam, C. Y.; Chen, G. H. J. *Chem. Phys.* **2007**, *126*, 244102.

(20) (a) Nakano, M.; Ohta, S.; Kishi, R.; Nate, M.; Takahashi, H.; Furukawa, S.-i.; Nitta, H.; Yamaguchi, K. *J. Chem. Phys.* **2006**, *125*, 234707. (b) Nakano, M.; Kishi, R.; Minami, T.; Fukui, H.; Nagai, H.; Yoneda, K.; Takahashi, H. *Chem. Phys. Lett.* **2008**, *460*, 370. (c) Kishi, R.; Nakano, M.; Minami, T.; Fukui, H.; Nagai, H.; Yoneda, K.; Takahashi, H. *J. Phys. Chem. A* **2009**, *113*, 5455.
(21) (a) Kishi, R.; Nakano, M.; Minami, T.; Fukui, H.; Nagai, H.; Yoneda, K.; Takahashi, H. *Synth. Met.* **2009**, *159*, 2194. (b) Kishi, R.; Minami, T.; Fukui, H.; Takahashi, H.; Nakano, M. *J. Chem. Phys.* **2008**, *128*, 244306. (c) Nakano, M.; Kishi, R.; Minami, T.; Yoneda, K. *Molecules* **2009**, *14*, 3700.
(22) Kishi, R.; Nakano, M. *J. Phys. Chem. A* **2011**, *115*, 3565.
(23) (a) Nakano, M.; Shigemoto, I.; Yamanaka, S.; Yamaguchi, K. *J. Chem. Phys.* **1995**, *103*, 4175. (b) Nakano, M.; Yamada, S.; Shigemoto, I.; Yamaguchi, K. *Chem. Phys. Lett.* **1996**, *250*, 247. (c) Nakano, M.; Fujita, H.; Takahata, M.; Yamaguchi, K. *Chem. Phys. Lett.* **2002**, *356*, 462. (d) Nakano, M.; Fukui, H.; Minami, T.; Yoneda, K.; Shigeta, Y.; Kishi, R.; Champagne, B.; Botek, E.; Kubo, T.; Ohta, K.; Kamada, K. *Theor. Chem. Acc.* **2011**, *130*, 711. (e) Nakano, M.; Fukui, H.; Minami, T.; Yoneda, K.; Shigeta, Y.; Kishi, R.; Champagne, B.; Botek, E.; Kubo, T.; Ohta, K.; Kamada, K. *Theor. Chem. Acc.* **2011**, *130*, 725.
(24) Carmichael, H. J. *Statistical Methods in Quantum Optics 1*; Springer Verlag: Berlin, Germany, 1999.
(25) Leegwater, J. A.; Durrant, J. R.; Klug, D. R. *J. Phys. Chem. B* **1997**, *101*, 7205.
(26) (a) Nakano, M.; Takahata, M.; Fujita, H.; Kiribayashi, S.; Yamaguchi, K. *Chem. Phys. Lett.* **2000**, *323*, 249. (b) Takahata, M.; Nakano, M.; Fujita, H.; Yamaguchi, K. *Chem. Phys. Lett.* **2002**, *363*, 422.
(27) Willets, A.; Rice, J. E.; Burland, D. M.; Shelton, D. P. *J. Chem. Phys.* **1992**, *97*, 10.
(28) (a) Ye, A.; Autschbach, J. *J. Chem. Phys.* **2006**, *125*, 234101. (b) Ye, A.; Patchkovskii, S.; Autschbach, J. *J. Chem. Phys.* **2007**, *127*, 074104.
(29) Nakano, M.; Kishi, R.; Nakagawa, N.; Nitta, T.; Yamaguchi, K. *J. Phys. Chem. B* **2005**, *109*, 7631.
(30) Foresman, J. B.; Head-Gordon, M.; Pople, J. A.; Frisch, M. J. *J. Phys. Chem.* **1992**, *96*, 135.
(31) Frisch, M. J.; Trucks, G. W.; Schlegel, H. B.; Scuseria, G. E.; Robb, M. A.; Cheeseman, J. R.; Montgomery, J. A., Jr.; Vreven, T.; Kudin, K. N.; Burant, J. C.; Millam, J. M.; Iyengar, S. S.; Tomasi, J.; Barone, V.; Mennucci, B.; Cossi, M.; Scalmani, G.; Rega, N.; Petersson, G. A.; Nakatsuji, H.; Hada, M.; Ehara, M.; Toyota, K.; Fukuda, R.; Hasegawa, J.; Ishida, M.; Nakajima, T.; Honda, Y.; Kitao, O.; Nakai, H.; Klene, M.; Li, X.; Knox, J. E.; Hratchian, H. P.; Cross, J. B.; Bakken, V.; Adamo, C.; Jaramillo, J.; Gomperts, R.; Stratmann, R. E.; Yazyev, O.; Austin, A. J.; Cammi, R.; Pomelli, C.; Ochterski, J. W.; Ayala, P. Y.; Morokuma, K.; Voth, G. A.; Salvador, P.; Dannenberg, J. J.; Zakrzewski, V. G.; Dapprich, S.; Daniels, A. D.; Strain, M. C.; Farkas, O.; Malick, D. K.; Rabuck, A. D.; Raghavachari, K.; Foresman, J. B.; Ortiz, J. V.; Cui, Q.; Baboul, A. G.; Clifford, S.; Cioslowski, J.; Stefanov, B. B.; Liu, G.; Liashenko, A.; Piskorz, P.; Komaromi, I.; Martin, R. L.; Fox, D. J.; Keith, T.; Al-Laham, M. A.; Peng, C. Y.; Nanayakkara, A.; Challacombe, M.; Gill, P. M. W.; Johnson, B.; Chen, W.; Wong, M. W.; Gonzalez, C.; and Pople, J. A. *Gaussian 03*, revision C.02; Gaussian, Inc.: Wallingford, CT, 2004.
(32) Kamiya, M.; Sekino, H.; Tsuneda, T.; Hirao, K. *J. Chem. Phys.* **2005**, *122*, 234111.
(33) de Wergifosse, M.; Champagne, B. *J. Chem. Phys.* **2011**, *134*, 074113.